WATER RESOURCES RESEARCH, VOL. 35, NO. 8, PAGES 2313–2320, AUGUST 1999

Tidal water table fluctuations in a sandy ocean beach

B. Raubenheimer[1] and R. T. Guza
Center for Coastal Studies, Scripps Institution of Oceanography, La Jolla, California

Steve Elgar[1]
Electrical Engineering and Computer Science, Washington State University, Pullman

Abstract. Tidal water table fluctuations observed for 27 days in a gently sloped ocean beach are predicted well by numerical models based on the Boussinesq equation driven with the observed 10 min–averaged shoreline (ocean-beach intersection) motion. Diurnal and semidiurnal water table fluctuations are almost completely damped 100 m landward of the mean shoreline location on this fine-grained sand beach, but fluctuations at spring-neap periods (≈14 days) are attenuated less. Comparison of the observations with the predictions suggests that the asymmetries in the water table level time series measured in this study result from nonlinearity owing to the large (relative to the wavelength) horizontal shoreline excursions, rather than from nonlinearity owing to finite-amplitude water table fluctuations. Cross-shore variations of the aquifer depth are predicted to have a small effect on the landward decay rate of the water table fluctuations. The seepage face width is predicted accurately and depends on the nonplanar beach profile. In general, the development of a seepage face is predicted to have little effect on the water table level landward of the intertidal region.

1. Introduction

The elevation of the groundwater in a sandy beach is believed to be important to erosion [*Grant*, 1948; *Duncan*, 1964; *Eliot and Clarke*, 1988], saltwater intrusion [*Nielsen*, 1999], and biological activity [*Pollock and Hummon*, 1971; *McArdle and McLachan*, 1991]. Ocean tides drive fluctuations in the beach water table that decay landward from the shoreline (the beach-ocean intersection), are asymmetric and skewed (e.g., pitched forward and peaky) in time, and have average levels higher (overheight) than mean sea level [*Emery and Foster*, 1948; *Isaacs and Bascom*, 1949; *Lanyon et al.*, 1982]. When the tide falls more rapidly than the beach drains, a seepage face forms between the shoreline and the intersection of the water table with the beach (the "water table outcrop"), possibly enhancing sediment transport [*Turner*, 1993].

Numerical models based on the nonlinear (finite-amplitude) Boussinesq equation (appropriate for shallow aquifers) and initialized with water table fluctuations observed inland of the intertidal region, the area of the beachface alternately covered and uncovered by the ocean tides, accurately predict the amplitude and phase of tidal water table fluctuations farther landward [*Harrison et al.*, 1971; *Dominick et al.*, 1971; *Fang et al.*, 1972]. Recent studies have concerned processes within the intertidal region, which can be wide on beaches with gentle slopes or large tides. When the horizontal excursion of the shoreline location over a tidal period is significant, nonlinearity introduced at the shoreline affects the inland water table fluctuations. The nonlinearity parameters associated with the Boussinesq equation and the moving shoreline boundary condition are $\mu = A/D$ and $\varepsilon = kA \cot \beta$, respectively, where A and k are the vertical amplitude and wavenumber of the groundwater fluctuations, D is the (constant) aquifer thickness, and β is the (planar) beach slope.

Nielsen [1990] used analytic solutions of the Boussinesq equations to examine the effects of the moving shoreline on water table fluctuations. To simplify the equations, the aquifer thickness and beach slope were assumed to be constant, and the water table was assumed to intersect the beachface at the shoreline (e.g., no seepage face). When terms of order ε ($O(\varepsilon)$) are negligible (e.g., a steeply sloped beach), perturbation expansion of the nonlinear (finite-amplitude) Boussinesq equation gives (to $O(\mu)$)

$$\eta(x, t) = A \cos(\omega t - kx)e^{-kx} + \frac{\mu A}{4}[1 - e^{-2kx} + \cos(2\omega t - \sqrt{2}kx)e^{-\sqrt{2}kx} - \cos(2\omega t - 2kx)e^{-2kx}] \quad (1)$$

where ω is the radian frequency of the monochromatic (single-frequency) ocean tide and $\eta(x, t)$ represents deviations of the water table height at cross-shore position x and time t from the still height D (e.g., the total water table height $h(x, t) = \eta(x, t) + D$). In contrast, if terms of $O(\mu)$ are negligible, perturbation solutions of the linear (small-amplitude) Boussinesq equation are (to $O(\varepsilon)$)

$$\eta(x, t) = A \cos(\omega t - kx)e^{-kx} + \varepsilon A\left[\frac{1}{2} + \frac{\sqrt{2}}{2}\cos(2\omega t + \pi/4 - \sqrt{2}kx)e^{-\sqrt{2}kx}\right] \quad (2)$$

Thus the mean overheight of the water table could result from finite-amplitude tidal fluctuations (terms of $O(\mu)$) or from the moving shoreline (terms of $O(\varepsilon)$). The fluctuations of $O(\varepsilon)$ at harmonic frequencies (e.g., 2ω) in (2) are associated with the

[1]Now at Woods Hole Oceanographic Institution, Woods Hole, Massachusetts.

Paper number 1999WR900105.
0043-1397/99/1999WR900105$09.00

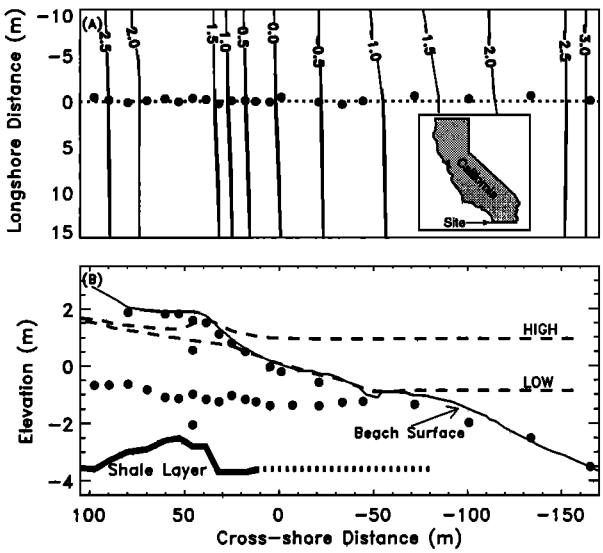

Figure 1. (a) Experiment plan view showing locations of pressure sensors (solid circles) and beach elevation contours (in meters relative to mean sea level). The cross-shore transect (dotted line) corresponds to the model trace. (b) Sensor locations, Torrey Pines Beach profile, and the envelope of water table and tidal levels (dashed curves). The thick solid and dotted curves at the bottom represent the measured upper surface of the Ardath Shale and the (unmeasured) offshore shale position, respectively, used in the finite-amplitude numerical model.

moving shoreline and propagate landward as damped free waves, satisfying the linear dispersion relation

$$k = \sqrt{\frac{n_e \omega}{2KD}} \tag{3}$$

where K is the hydraulic conductivity in the saturated beach and n_e is the effective porosity. In contrast, the terms of $O(\mu)$ in (1) result in harmonics at frequency 2ω with wavenumbers both of bound waves ($2k$) not satisfying the free wave dispersion relation (3) and of free waves ($\sqrt{2}k$). There is a similar generation of free harmonics by a moving boundary and of bound harmonics by nonlinearity away from the boundary when water waves are produced by sinusoidal oscillations of a wavemaker in a flume [*Madsen*, 1971].

The overheight, harmonic generation, and landward decay of fluctuations predicted by the analytic solution for small amplitude (2) agree roughly with observations collected over a tidal period [*Nielsen*, 1990]. Improved agreement is obtained with numerical solutions of the fully nonlinear Boussinesq equations (and extensions) [*Kang and Nielsen*, 1996; *Li et al.*, 1997a; *Baird et al.*, 1998]. However, the relative importance to tidal water table fluctuations of spatially variable aquifer depth, nonplanar bathymetry, development of the seepage face, and nonlinearity owing to finite amplitude and the moving shoreline are not understood well.

Here small-amplitude ($\mu \approx 0.2$) tidal water table fluctuations and seepage face locations measured continuously for 27 days (e.g., one lunar cycle) within a gently sloped natural beach with large shoreline excursions ($\varepsilon \geq 1$) are used to test further the Boussinesq equations. The observations and models are described in sections 2 and 3, respectively, and model predictions are compared with observations in section 4. Numerical simulations to assess different model terms and to study harmonic generation in the intertidal region are described in section 5.

2. Observations

Waves, tides, and water table fluctuations were sampled nearly continuously at 2 Hz (real-time frequency) from September 18 to October 14, 1996, at Torrey Pines Beach, California (Figure 1). Surf zone waves were measured with 16 pressure sensors located near the sand surface, and water table fluctuations were measured with 22 buried pressure sensors. Wave and water table sensors were stacked vertically to estimate vertical infiltration and to detect capillary effects [*Gillham*, 1984; *Turner and Nielsen*, 1997]. Beach surface profile changes, calculated from daily surveys to ~2-m water depth, were small (<10 cm) both in the intertidal region ($-40 \leq x < 39$ m in Figure 1b) and landward. At the beginning, middle, and end of the experiment the profile was measured landward of ~5-m water depth. The average beach slope over the intertidal region was ~0.03, with slopes of 0.05 landward and 0.02 seaward of $x = 0$ m, defined as the intersection of the beach profile and the experiment-averaged offshore sea level. Offshore wind wave heights measured in 10-m water depth ~35 km north of the experiment site ranged from 40 to 90 cm, and peak periods ranged from 8 to 20 s. No rainfall was recorded.

At 15 locations between cross-shore distances 10 and 100 m, 8-m deep holes were drilled to collect sediment cores and to determine the beach stratigraphy. Sieve analysis was conducted on 11 cores to determine grain sizes, and five cores were used to determine the porosity and permeability of the beach sedimentary layers. The analysis suggested that the beach is composed of ~2–4 m of uniform fine to medium sand with traces of silt ($d_{50} \approx 0.23$ mm, porosity ≈37%, and hydraulic conductivity ≈0.07 cm s^{-1}) overlying ~1 m of Scripps formation composed of dense, silty fine sand with traces of gravel ($d_{50} \approx 0.15$ mm, porosity ≈33%, and hydraulic conductivity ≈0.03 cm s^{-1}) on top of low-permeability Ardath Shale ($d_{50} \approx 0.004$ mm, porosity ≈32%, and hydraulic conductivity ≈0.0005 cm s^{-1}). The average hydraulic conductivity of the unconfined aquifer, estimated from slug tests [*Bouwer and Rice*, 1976; *Brown and Narasimhan*, 1995] conducted at cross-shore distances 60 and 91 m, was 0.07 cm s^{-1}. All pressure sensors were located above the Scripps formation.

Experiment mean water table levels (Figure 2a) are higher than mean sea level at all locations and increased landward (because of an inland water source and nonlinearly driven overheight, e.g., (1) and (2)). Offshore tidal amplitudes ranged from ~50 cm during neap tides to 100 cm during spring tides (Figure 2b). Diurnal and higher-frequency tidal water table fluctuations decay landward (analogous to the conductive penetration of surface heat) and are almost completely damped 98 m onshore of the mean shoreline, but fluctuations at the frequency of the spring-neap tidal cycle are attenuated less (Figure 2a). Spring-neap water table fluctuations have not been observed previously, probably because most observations spanned only a few days. Ocean water level and beach water table fluctuations are dominated by tides with 25- and 12-hour periods (Figures 2b and 3). The water table spectra also contain peaks at higher-frequency harmonics (e.g., at multiples and combinations of the diurnal and semidiurnal frequencies). The magnitudes of water table fluctuations at all frequencies decay landward ($x > 39$ m) of the intertidal region. Within

the intertidal region, energy with 6-, 8-, 12-, and 25-hour periods reaches a maximum near the mean shoreline location, and energy at 4- and 5-hour periods reaches a maximum farther landward near cross-shore distance 39 m (Figure 3).

3. Numerical Models

The Boussinesq equation for finite-amplitude (nonlinear) water table fluctuations and spatially variable aquifer thickness $D(x)$ is

$$\frac{\partial \eta(x, t)}{\partial t} = \frac{K}{n_e} \frac{\partial}{\partial x} \left\{ [D(x) + \eta(x, t)] \frac{\partial \eta(x, t)}{\partial x} \right\} \quad (4)$$

For small-amplitude (linear) water table fluctuations and constant aquifer depth the Boussinesq equation becomes

$$\frac{\partial \eta(x, t)}{\partial t} = \frac{KD}{n_e} \frac{\partial^2 \eta(x, t)}{\partial x^2} \quad (5)$$

Following *Liu and Wen* [1997], (4) and (5) were solved numerically using a centered finite difference method in space and a fourth-order Runga-Kutta integration technique in time. The seaward boundary condition for the numerical solutions is

$$\eta(x_s, t) = z_s \quad (6)$$

where x_s and z_s are the horizontal location and the elevation, respectively, of the shoreline at time t. Perturbation solutions to (4) and (5), assuming constant beach slope, constant aquifer depth, and monochromatic ocean tides, are given by (1) and (2), respectively.

The Boussinesq equation is based on the assumptions that the sand drains instantaneously (e.g., no capillary fringe), density gradients are negligible, and horizontal flows are much larger than vertical flows. Tension heads observed with pressure sensors near the sand surface suggest that the capillary fringe extended ~50 cm above the water table level. However, capillary effects are believed to have little influence on water table fluctuations at tidal frequencies [*Barry et al.*, 1996; *Li et al.*, 1997b]. Density gradients owing to freshwater landward of the beach berm and saline ocean water in the intertidal region have been observed previously [*Harrison et al.*, 1971; *Nielsen*, 1999]. Densities were not measured in the present experiment, but the good agreement of the observed tidal water table levels with the predictions described below suggests that density effects were small. Horizontal flows usually are much larger than vertical flows (see the appendix) on the 10-min to 14-day timescales considered here, consistent with the model assumptions.

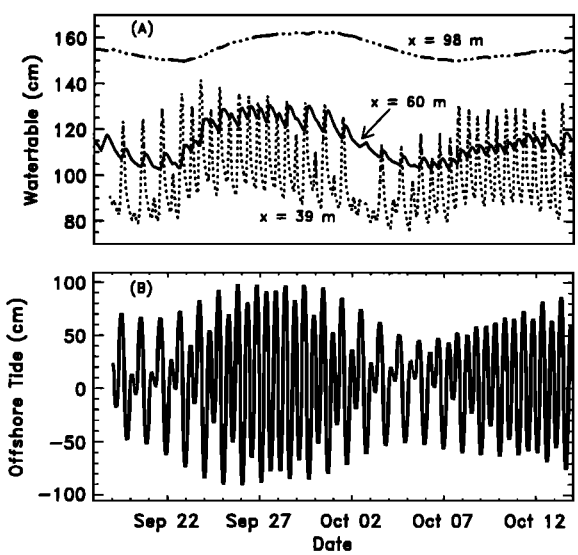

Figure 2. Observed (a) 10 min–averaged water table fluctuations (relative to mean sea level) at cross-shore distances 98, 60, and 39 m, and (b) offshore 34 min–averaged sea surface levels versus time.

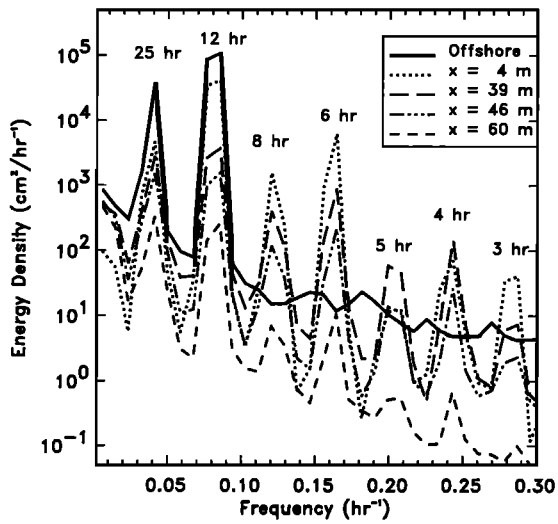

Figure 3. Energy density spectra (12 degrees of freedom) of observed offshore water level fluctuations and water table fluctuations at cross-shore distances 4, 39, 46, and 60 m.

In the finite-amplitude variable–aquifer depth model (4) the bottom boundary was at the top of the Ardath Shale (Figure 1b). In the small-amplitude constant–aquifer depth model (5) the bottom boundary was at the average (over the model domain) level of the shale layer ($z = -3.5$ m), and D was set equal to 4.7 m, the time- and space-averaged observed water table height. Above the impermeable boundary the beach material was assumed to be homogeneous and isotropic, with an average hydraulic conductivity K equal to 0.07 cm s^{-1}. The effective porosity n_e equaled 0.215, determined using a least squares fit of the finite-amplitude model predictions to the measured water level changes. The inland propagation of water table fluctuations and the seepage face width predicted using (4) and (5) depend on the ratio K/n_e [e.g., *Baird et al.*, 1998], so different values of K changed the corresponding best fit value of n_e but did not alter the agreement between observations and predictions. The models were initialized with the water table level observed at the start of the experiment. Initial levels onshore of the most landward sensor were estimated using a natural cubic spline extrapolation. Predicted water table fluctuations were negligibly small at the inland boundary (located 250 m onshore of the mean shoreline), where a constant seawater head (Dirichlet) condition was imposed. Increasing (decreasing) the head (2.55 m above mean sea level) at the model inland boundary by 40% results in an 8% increase (5% decrease) of the seepage face width and a 14% decrease (14% increase) of the water table fluctuation amplitudes inland of the maximum shoreline location.

The locations of the shoreline and the water table outcrop at the sand surface were estimated using observations made with the closely spaced sensors in the intertidal region and the

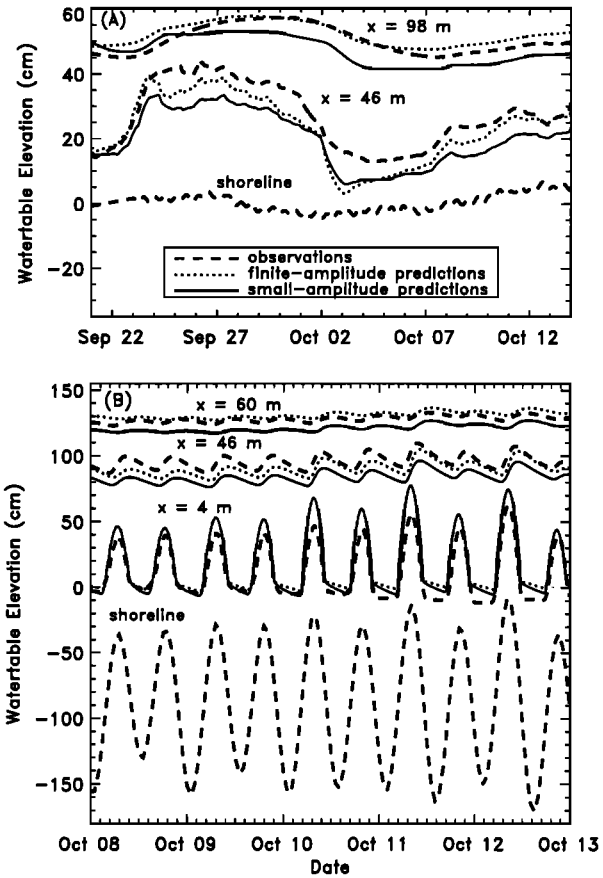

Figure 4. Water table and shoreline fluctuations versus time: (a) 25 hour–averaged for 24 days at cross-shore distances 46 and 98 m and (b) 10 min–averaged for 5 days at cross-shore distances 4, 46, and 60 m. Observations and small- and finite-amplitude predictions at each location are relative to an arbitrary datum.

measured beach profile. The cross-shore structure of the mean water surface was estimated by fitting a cubic spline to 10 min–averaged water levels. Sand level was determined by fitting a cubic spline to the initial beach profile. Because of inaccuracies in the mean water levels and beach profiles, the shoreline location was defined as the most offshore location where the water depth above the beach profile was less than a small number δ_s. The water table outcrop location was estimated as the most landward position where the water table was less than δ_w below sand level. The results were insensitive to variation of δ_s and δ_w between 1 and 5 cm and to the $O(10$ cm) changes in the beach profile that occurred during the experiment. In the results discussed below, $\delta_s = \delta_w = 2$ cm. At low tide, when the beach was saturated, the 10 min–average shoreline was near the maximum wave runup location in that 10-min period, whereas at high tide the shoreline was near the water table outcrop because waves extending farther landward infiltrated into the dry sand. This shoreline definition, suggested by *Nielsen* [1989], resulted in a skewing of the shoreline time series and therefore in spectral peaks at harmonic frequencies. However, water table predictions obtained by driving the model with the total ($f \leq 3.00$ h^{-1}, containing all harmonics) and with low pass–filtered ($f \leq 0.11$ h^{-1}, no harmonics) shoreline time series were similar. In the results shown below the seaward model boundary condition (6) was located at the observed low-passed ($f \leq 0.11$ h^{-1}) shoreline location.

4. Model-Data Comparisons

The water table observations are predicted well by both numerical models (Figure 4), suggesting that for the hydrologic conditions considered here, nonlinearities are unimportant inland of the moving shoreline. The average (over 27 days) errors of the small- and finite-amplitude model predictions are <10 cm. The largest mean errors are underprediction of the average water table levels in the intertidal region. The standard deviations (e.g., mean errors removed) of differences between the observations and the small- and finite-amplitude model predictions are <4 and 3 cm, respectively.

The magnitudes of the spring-neap tidal cycle near the berm ($x = 46$ m, Figure 4a) are similar to a time-modulated tidal overheight. However, the observed and predicted spring-neap water table fluctuation amplitudes decrease landward with an increasing phase lag (compare $x = 46$ with $x = 98$ m in Figure 4a). The landward amplitude decay also is predicted by perturbation solutions (not shown) to (5) for multifrequency shoreline excursions. When ocean tides are assumed to be bichromatic with energy at frequencies ω and $\omega + \delta\omega$ (e.g., shoreline fluctuations at semidiurnal solar (12.00 hour) and lunar (12.42 hour) tidal periods), groundwater fluctuations of $O(\varepsilon)$ include free waves at the difference frequency $\delta\omega$ (e.g., spring-neap periods) as well as at the sum frequencies 2ω, $2\omega + \delta\omega$, and $2\omega + 2\delta\omega$.

The numerical models accurately predict the water table fluctuations at diurnal and higher tidal frequencies (Figure 4b), including the observed frequency-dependent landward decay and increasing phase lags (Figure 5). The observed slow drainage of the beach at low tide, which causes skewed (e.g., peaky) and asymmetric (e.g., pitched forward) water level fluctuation time series, is predicted well (e.g., $x = 4$ and 46 m in Figure 4b). The observed and predicted skewness and asymmetry of the water table fluctuations increase across the intertidal region, reaching maximum values near the berm before decreasing landward (Figure 6).

On the falling tide the formation of a seepage face between the water table outcrop and the shoreline is predicted by both numerical models (Figure 7). The water table outcrop location is predicted accurately by the finite-amplitude model but is too far seaward in the small-amplitude model, so the observed seepage face width (average value 10 m) is underestimated. Average (± standard deviation) differences between observed and predicted seepage face widths are 0.3 ± 4.4 and −1.8 ± 4.3 m for the finite- and small-amplitude models, respectively.

Previous studies have suggested that the seepage face width on macrotidal beaches can be estimated by assuming that the water table outcrop position is independent of the pressure distribution within the beach and depends only on the rate that the tide falls, the beach slope, and K/n_e [*Dracos*, 1963; *Turner*, 1993]. However, this simple model and the present outcrop observations agree only if the ratio K/n_e is increased unrealistically (by a factor of 8) relative to that used in the numerical Boussinesq model. Furthermore, model simulations (not shown) suggest that the seepage face width is sensitive to the head (or hydraulic gradient) at the model inland boundary. Consistent with previous observations [*Turner*, 1993], the predicted seepage face width depends on the beach geometry. The average seepage face width predicted numerically on a planar

beach with a slope equal to the average observed intertidal slope (0.031) is <~1 m (not shown), approximately one-tenth that predicted using the observed profile. *Nielsen* [1990] speculated that underprediction of the asymmetry by (2) resulted from the neglect of a seepage face. However, inland ($x > 39$ m) of the intertidal region, the amplitude decay rate, phase lags, skewness, and asymmetry of water table fluctuations predicted on planar and measured profiles are insensitive (differences are less than 1, 1, 3, and 6%, respectively) to the substantially different seepage face widths.

5. Discussion

5.1. Nonlinearity and Aquifer Depth

The predictions of the finite-amplitude variable–aquifer depth and small-amplitude constant–aquifer depth models are similar (Figures 4–7), suggesting that the effects of variable aquifer thickness (the deviation of the shale layer from horizontal, Figure 1b) and nonlinearity in the Boussinesq equation are not large for conditions similar to those observed here. Although small, the effect of variable aquifer thickness in the model simulations is detectable. Landward of the intertidal region, the small-amplitude model predicts that all frequency components propagate as free waves

$$\eta(x, t) = Ae^{-k_R x} \cos(\omega t - k_I x) \quad (7)$$

where k_R and k_I are the real and imaginary parts of the wavenumber, respectively, and are given by $k_R = k_I = k$ (e.g., (3)). Values of k given analytically by (3) differ by <1% from values of k_R and k_I obtained by fitting (7) to the numerical small-amplitude model (5) predictions, confirming the accuracy of the numerical solution. The k_R and k_I estimated by fitting (7) to the observations and to the finite-amplitude model (4) predictions are similar to the analytic (and equivalent small-amplitude model) values (compare open and solid symbols, respectively, with the solid curve in Figure 8a). However, at fixed frequency the observed and finite-amplitude k_R are larger than the k_I. Retaining finite amplitude but assuming constant aquifer depth in the finite-amplitude model yields $k_R \approx k_I \approx k$ (Figure 8b), indicating that differences between the finite- and small-amplitude model predictions are caused primarily by the variable aquifer depth, rather than by nonlinearity.

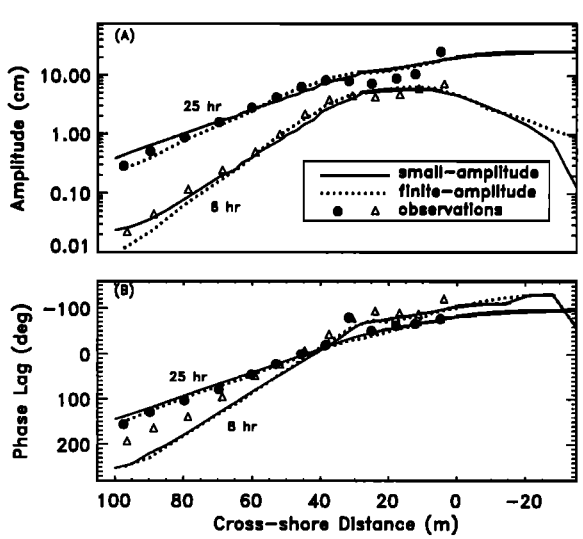

Figure 5. (a) Amplitudes and (b) phase lags (with respect to observations at $x = 46$ m) of water table fluctuations with periods of 25 and 8 hours versus cross-shore distance. Observed values and small- and finite-amplitude-model-predicted values are calculated using cross spectra with 36 degrees of freedom (dof). Results for 12- and 6-hour periods (not shown) are similar.

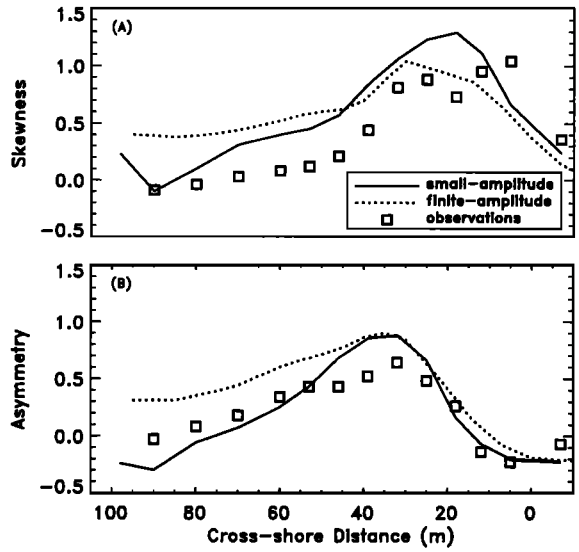

Figure 6. (a) Skewness and (b) asymmetry of measured and small- and finite-amplitude-model-predicted water table fluctuations versus cross-shore distance.

Differences between the observations and model predictions at 6- and 8-hour periods may be caused by either an intermediate-depth ($0.2 < n_e\omega D/K < 1.0$) aquifer [*Parlange et al.*, 1984; *Nielsen et al.*, 1996; *Liu and Wen*, 1997] or the capillary fringe [*Barry et al.*, 1996; *Li et al.*, 1997b]. Small-amplitude intermediate depth–aquifer solutions [*Nielsen et al.*, 1996] yield $k_R = 0.085$ and $0.099\ m^{-1}$ and $k_I = 0.077$ and $0.087\ m^{-1}$ for frequencies $f = 0.12$ and $0.16\ hr^{-1}$, respectively. At lower frequencies, where the effect of finite aquifer depth is small (and the agreement between the observations and predictions

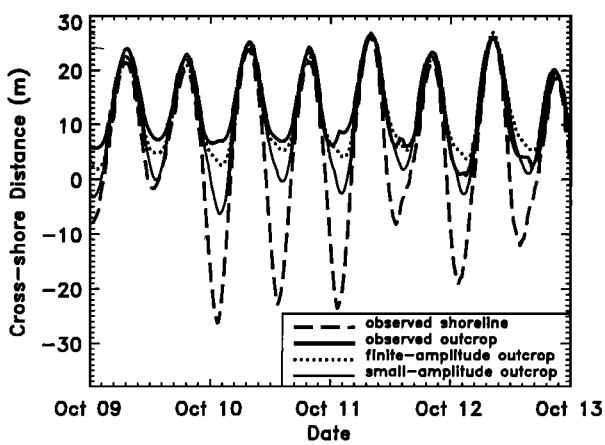

Figure 7. Cross-shore location of the observed 10 min–averaged shoreline and water table outcrop and of the water table outcrop predicted with the finite- and small-amplitude numerical models versus time. The seepage face is located between the shoreline and the water table outcrop.

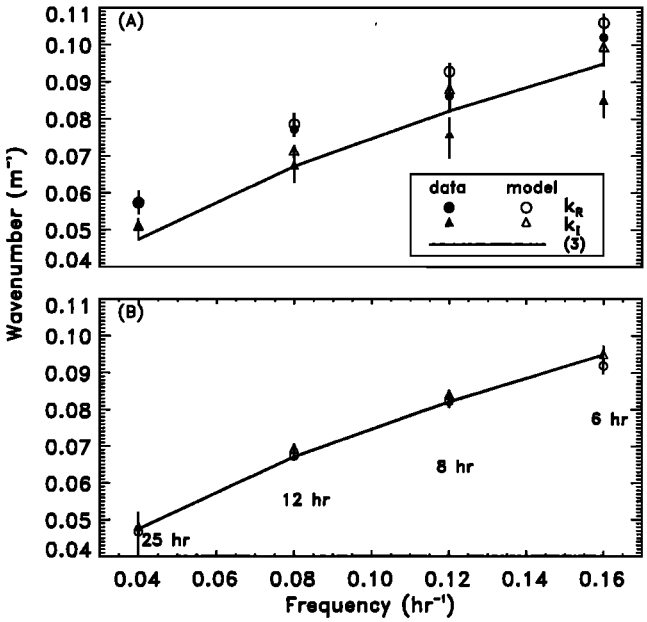

Figure 8. Real (k_R) and imaginary (k_I) part of the wavenumber estimated using (a) observations and finite-amplitude variable–aquifer depth predictions and (b) finite-amplitude constant–aquifer depth predictions versus frequency. Vertical bars represent the 99% confidence limits.

is good), variable aquifer depth likely contributes to the differences between observed k_R and k_I.

5.2. Moving Shoreline

The generation by the moving shoreline of energy at tidal harmonics was investigated by comparing numerical model predictions driven with shoreline time series band passed to include energy having only a diurnal (25 hour, e.g., $0.02 \leq f \leq 0.06$ h^{-1}) or semidiurnal ($0.06 \leq f \leq 0.10$ h^{-1}) period with predictions driven with combined diurnal and semidiurnal ($0.02 \leq f \leq 0.10$ h^{-1}) shoreline fluctuations. Differences in the model predictions at tidal harmonic periods (e.g., 8, 6, 5, 4, and 3 hours) are ascribed to the (nonlinear) effect of energy at the period neglected in the shoreline boundary condition. Consistent with the analytical solution (2) for a sloping beach, water table fluctuations are generated at harmonics (e.g., integer multiples) of the frequencies of the peak shoreline fluctuations (Figure 9). The magnitude of spectral levels at 6- and 4-hour periods with semidiurnal forcing alone are similar to those predicted with combined forcing (compare dashed with solid curves in Figure 9), suggesting that these energy peaks are harmonics of the semidiurnal tide. However, the energy levels at 8-, 5-, and 3-hour periods predicted with only diurnal forcing are reduced substantially relative to those predicted with combined forcing (compare dotted with solid curves in Figure 9), suggesting that energy at these periods is generated by nonlinear sum interactions between diurnal and semidiurnal shoreline fluctuations.

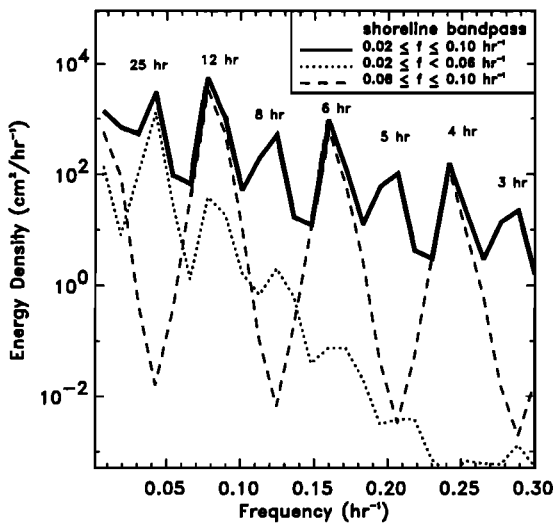

Figure 9. Energy density spectra of finite amplitude–predicted water table fluctuations at a cross-shore distance of 35 m. The model was driven with band-passed observed shoreline time series. Small-amplitude model predictions (not shown) are similar, so only finite-amplitude model results are shown. Numbers above each spectral peak indicate the approximate period.

6. Summary

Tidal water table levels were observed on an ocean beach with large (relative to the wavelength, $\varepsilon \geq 1$) horizontal shoreline excursions. Similar to previous observations, water table fluctuations decrease landward with increasing phase lags and are asymmetric and skewed in time (Figures 2–6). Although diurnal and semidiurnal water table fluctuations are almost completely damped 100 m landward of the mean shoreline location, fluctuations at spring-neap periods (≈14 days) are attenuated less (Figures 2 and 4). The observed fluctuations are described well (Figures 4–6) by both finite-amplitude variable–aquifer depth (4) and small-amplitude constant–aquifer depth (5) numerical Boussinesq models. The moving shoreline, included in both models, results in the generation of harmonic fluctuations (Figure 9). For the hydraulic conditions considered here, nonlinearities are unimportant inland of the intertidal region, and water table fluctuations propagate as free waves approximately satisfying the dispersion equation (3) based on the linear (small-amplitude) Boussinesq equation with a constant aquifer depth (Figure 8). Cross-shore variations of the aquifer depth, neglected in (3), cause small but detectable differences between the predicted real and imaginary parts of the wavenumber. Development of a seepage face (Figure 7) and nonplanar beach bathymetry are predicted to have little effect on inland water table fluctuations. Additional observations and modeling are needed to generalize these results to beaches with properties (e.g., slope, hydraulic conductivity, porosity, aquifer depth, and hydraulic gradient) and tidal ranges different than those considered here.

Appendix: Horizontal and Vertical Flows

The horizontal u and vertical w flows through saturated sand beneath the berm and intertidal zone are estimated using gradients of observed 10 min–averaged pressure heads ($p_w + z_R \rho g$, where p_w is measured pressure, z_R is the vertical sensor location relative to a fixed datum, ρ is the ocean water density, and g is gravitational acceleration) and Darcy's law for laminar flow,

$$u = +\frac{K}{N}\frac{\partial(p_w/\rho g - z_R)}{\partial x} \qquad \text{(A1)}$$

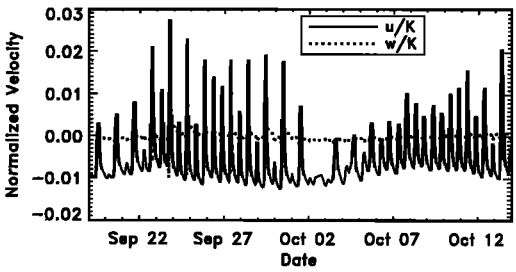

Figure A1. Horizontal (u) and vertical (w) velocities normalized by hydraulic conductivity K versus time. Velocities were estimated using 10 min–averaged pressure gradients measured with horizontally ($x = 39$ and 53 m at $z = -1.1$ m) and vertically ($z = 0.6$ and -2.2 m at $x = 46$ m) separated sensors (Figure 1b). Negative horizontal and vertical flows are landward and downward, respectively.

$$w = -\frac{K}{N}\frac{\partial(p_w/\rho g - z_R)}{\partial z} \tag{A2}$$

where z is vertical distance positive upward. Horizontal flows are usually much larger than vertical flows, consistent with the model assumptions. For instance, beneath the berm (where pressure gradients can be estimated at all tidal stages using deeply buried stacked sensors, $x = 46$ m in Figure 1b) the horizontal velocities are typically ~10 times larger than the vertical velocities (Figure A1). Relatively large vertical velocities occur during spring high tides (e.g., see dotted line, Figure A1, September 23) when the sensors were beneath the swashzone (the area of the beachface alternately covered and uncovered by waves), but horizontal flows are greater than vertical flows more than 95% of the time.

Offshore of the berm and onshore of the shoreline, where only two sensors are stacked vertically, vertical flows are estimated only when the water table level is higher than the upper "wave" sensor elevation (located near sand level, Figure 1b). Thus these intertidal flow estimates are restricted to times when the upper sensor was beneath the seepage face or the swashzone. Corresponding horizontal flows are estimated using the lower water table and adjacent onshore sensor. Although vertical flows are expected to be largest for this subset of the observations (e.g., Figure A1), the geometric average of the flow ratio (u/w) never is <1 and usually is >4. Vertical velocities were greater than horizontal velocities in 42% of the estimates at one swashzone location ($x = 32$ m), but at most locations, relatively large vertical flows occurred in <7% of the estimates.

Notation

A shoreline fluctuation amplitude.
D constant aquifer thickness.
$D(x)$ spatially variable aquifer thickness.
ε shoreline parameter.
f frequency.
g gravitational acceleration.
$\eta(x, t)$ water table elevation.
$h(x, t)$ total water table height ($\eta(x, t) + D(x)$).
K hydraulic conductivity.
k wavenumber.
k_R real part of wavenumber.
k_I imaginary part of wavenumber.
μ nonlinearity parameter.
n_e effective porosity.
p_w pressure.
ρ density.
t time.
u horizontal flow.
w vertical flow.
ω wave frequency (radians).
x cross-shore distance.
x_s horizontal shoreline location.
z depth below sand surface.
z_s shoreline elevation.
z_r sensor elevation.

Acknowledgments. This research was supported by the Office of Naval Research, the National Science Foundation, the Mellon Foundation, and the Naval Research Laboratory. Staff from the Center for Coastal Studies deployed and maintained the nearshore instruments. Offshore wave information was provided by the Coastal Data Information Program. The cooperation of the staff at Torrey Pines State Park is gratefully acknowledged. The authors thank the anonymous reviewers and R. Hanson for their helpful comments.

References

Baird, A. J., T. Mason, and D. P. Horn, Validation of a Boussinesq model of beach ground water behavior, *Mar. Geol., 148*, 55–69, 1998.

Barry, D. A., S. J. Barry, and J.-Y. Parlange, Capillary correction to periodic solutions of the shallow flow approximation, in *Mixing in Estuaries and Coastal Seas, Coastal Estuarine Stud.*, vol. 50, edited by C. B. Pattiaratchi, pp. 496–510, AGU, Washington, D. C., 1996.

Bouwer, H., and R. C. Rice, A slug test for determining hydraulic conductivity of unconfined aquifers with completely or partially penetrating wells, *Water Resour. Res., 12*, 423–428, 1976.

Brown, D. L., and T. N. Narasimhan, An evaluation of the Bouwer and Rice method of slug test analysis, *Water Resour. Res., 31*, 1239–1246, 1995.

Dominick, T. F., B. Wilkins, and H. Roberts, Mathematical model for beach groundwater fluctuations, *Water Resour. Res., 7*, 1626–1635, 1971.

Dracos, T., Ebene nichtstationare Grundwasserabflusse mit freier Oberflache, *Rep. 57*, 114 pp., Swiss Fed. Tech. Lab. Hydraul. Res. Soil Mech., Zürich, Switzerland, 1963.

Duncan, J. R., The effects of watertable and tide cycle on swash-backwash sediment distribution and beach profile development, *Mar. Geol., 2*, 186–197, 1964.

Eliot, I. G., and D. J. Clarke, Semi-diurnal variation in beachface aggradation and degradation, *Mar. Geol., 79*, 1–22, 1988.

Emery, K. O., and J. F. Foster, Watertables in marine beaches, *J. Mar. Res., 7*, 644–654, 1948.

Fang, C. S., S. N. Wang, and W. Harrison, Groundwater flow in a sandy tidal beach, 2, Two-dimensional finite element analysis, *Water Resour. Res., 8*, 121–128, 1972.

Gillham, R. W., The capillary fringe and its effect on watertable response, *J. Hydrol., 67*, 307–324, 1984.

Grant, U. S., Influence of the watertable on beach aggradation and degradation, *J. Mar. Res., 7*, 655–660, 1948.

Harrison, W., C. S. Fang, and S. N. Wang, Groundwater flow in a sandy tidal beach, 1, One dimensional finite element analysis, *Water Resour. Res., 7*, 1313–1322, 1971.

Isaacs, J. D., and W. N. Bascom, Water table elevations in some Pacific coast beaches, *Eos Trans. AGU, 30*, 293–294, 1949.

Kang, H.-Y., and P. Nielsen, Watertable dynamics in coastal areas, paper presented at 25th International Conference on Coastal Engineering, Am. Soc. of Civ. Eng., Orlando, Fla., 1996.

Lanyon, J. A., I. G. Eliot, and D. J. Clarke, Groundwater variation during semi-diurnal spring tidal cycles on a sandy beach, *Aust. J. Mar. Freshwater Res., 33*, 377–400, 1982.

Li, L., D. A. Barry, and C. B. Pattiaratchi, Numerical modeling of tide-induced beach water table fluctuations, *Coastal Eng., 30*, 105–123, 1997a.

Li, L., D. A. Barry, J.-Y. Parlange, and C. B. Pattiaratchi, Beach

watertable fluctuations due to wave run-up: Capillarity effects, *Water Resour. Res.*, *33*, 935–945, 1997b.

Liu, P. L.-F., and J. Wen, Nonlinear diffusive surface waves in porous media, *J. Fluid Mech.*, *347*, 119–139, 1997.

Madsen, O. S., On the generation of long waves, *J. Geophys. Res.*, *76*, 8672–8683, 1971.

McArdle, S. B., and A. McLachan, Dynamics of the swash zone and effluent line on sandy beaches, *Mar. Ecol. Prog. Ser.*, *76*, 91–99, 1991.

Nielsen, P., Wave setup and runup: An integrated approach, *Coastal Eng.*, *13*, 1–9, 1989.

Nielsen, P., Tidal dynamics of the water table in beaches, *Water Resour. Res.*, *26*, 2127–2134, 1990.

Nielsen, P., Groundwater dynamics and salinity in coastal barriers, *J. Coastal Res.*, in press, 1999.

Nielsen, P., R. Aseervatham, J. D. Fenton, and P. Perrochet, Groundwater waves in aquifers of intermediate depth, *Adv. Water Res.*, *20*, 37–43, 1996.

Parlange, J.-Y., F. Stagnitti, J. L. Starr, and R. D. Braddock, Free-surface flow in porous media and periodic solution of the shallow flow approximation, *J. Hydrol.*, *70*, 251–263, 1984.

Pollock, L. W., and W. D. Hummon, Cyclic changes in interstitial water content, atmospheric exposure, and temperature in a marine beach, *Limnol. Oceanogr.*, *16*, 522–535, 1971.

Turner, I. L., Watertable outcropping on macrotidal beaches: A simulation model, *Mar. Geol.*, *115*, 227–238, 1993.

Turner, I. L., and P. Nielsen, Rapid water table fluctuations within the beach face: Implications for swash zone sediment mobility?, *Coastal Eng.*, *32*, 45–59, 1997.

S. Elgar, Electrical Engineering and Computer Science, Washington State University, Pullman, WA 99164.

R. T. Guza and B. Raubenheimer, Center for Coastal Studies 0209, Scripps Institution of Oceanography, La Jolla, CA 92093. (britt@whoi.edu)

(Received October 15, 1998; revised March 25, 1999; accepted March 29, 1999.)